Palau Modeling Final Report

William Skirving, Scott Heron, Craig Steinberg,
Alan E. Strong, Cary McLean, Mal Heron,
Severine Choukroun, Felipe Arzayus & Andrew Bauman

The Nature Conservancy
SAVING THE LAST GREAT PLACES ON EARTH

MBA Financial Services

NOAA
NATIONAL OCEANIC AND ATMOSPHERIC ADMINISTRATION
U.S. DEPARTMENT OF COMMERCE

Australian Government

AUSTRALIAN INSTITUTE OF MARINE SCIENCE

Palau Modeling Final Report

William Skirving[1,3], Scott Heron[1,3], Craig Steinberg[2], Alan E. Strong[1], Cary McLean[2], Mal Heron[4], Severine Choukroun[2,4], Felipe Arzayus[1] and Andrew Bauman[5]

[1]NOAA/NESDIS Coral Reef Watch project, Silver Spring, MD, USA
[2]Australian Institute of Marine Science, Townsville, QLD, Australia
[3]Queensland Science and Engineering Consultants, Townsville, QLD, Australia
[4]School of Mathematical and Physical Sciences, JCU, QLD, Australia
[5]Office of Environmental Response and Coordination, Palau

Executive Summary

During the latter half of 1998, Palau experienced unprecedented bleaching that resulted in significant mortality and the loss of significant proportions of one of the few remaining pristine coral reefs in the world. Prior to 1998 and since 1998, little to no coral bleaching has been observed. These observations have been mirrored in the NOAA Coral Reef Watch DHW satellite DHW product. The DHW satellite product clearly shows that the 1998 accumulated stress easily surpassed the critical DHW=4 mark and is the only year to have done so since 1985, which is consistent with the field observations of bleaching.

The Nature Conservancy and the Palau Government have joined forces to design and implement a protected areas network (PAN) for Palau's coral reef ecosystem. They recognized bleaching as being potentially one of the major future threats to the Palau coral reef ecosystem, but with only one poorly documented bleaching event to go by, it is difficult to gain enough experience about the response of the ecosystem to this type of event to be able to build resilience to these events into the PAN.

In parallel with the PAN, NOAA and AIMS were collaborating on the development of the use of hydrodynamic models to predict heat stress during a bleaching event. In 2003, it was decided to combine these efforts and for NOAA and AIMS to produce a heat stress model for Palau for use in the PAN in an attempt to build in resilience against potential changes to future climate, regardless of the change.

For the model to be constructed, NOAA and AIMS needed:

1) The Palau bathymetry: Due to a lack of available conventional data, NOAA derived the bathymetry from a combination of Landsat data and *in situ* bathymetry transects taken with a depth sounder from a small boat. This produced a chart with 250 meter horizontal resolution and an RMS precision of ±1 meter vertically.

2) Low frequency currents: A combination of the Navy Research Laboratory's (NRL) Navy Layered Ocean Model (NLOM) and NOAA's Ocean Surface Current Analyses – Real time (OSCAR) were used to derive the seasonal low frequency currents around Palau.
3) High frequency currents: A combination of tide gauge data collected in and around Palau was used to derive a model that could accurately predict the tides. The bathymetry and the tidal model were then input into the Princeton Ocean Model (POM) to build a model of tidally induced currents in and around Palau. Field data collected over a period of 5 months were used to calibrate and validate the output of this model.
4) Vertical temperature profile: This was derived by modeling a patch of water with a homogeneous temperature and applying a diurnal cycle of solar radiation for a period of two weeks.
5) Validation data: This was derived from an intensive field deployment of current meters, temperature loggers, salinity loggers and tide gauges. This deployment has been documented in the Field Data Report, and is attached to this report as Appendix 1.

Using the bathymetry and low/high frequency currents as boundary conditions, a high resolution (250 m) two-dimensional (2-D) hydrodynamic model of the Palau region was developed to provide currents for the development of a heat stress map. The field validation data were used to assess the accuracy of the model and verified that the model was performing remarkably well, given the extremely large range of currents driven by tides within Palau.

Simpson and Hunter (1974) provide the parameterization that was used to distinguish between stratified and well-mixed water by combining the currents with the bathymetric data. This information was then used in conjunction with the vertical temperature profile to determine the likely spatial distribution of sea surface temperature. Although good approximations, these temperatures are better used as indications of spatial patterns of relatively cooler and warmer waters during a bleaching event. In fact, this model is more accurately characterized as a measure of thermal capacitance than temperature. The warmer regions have a low thermal capacitance and will heat up (and cool down) much faster than the cooler regions within the model, which have a much higher thermal capacitance.

The result of this is that the cooler regions in this model represent regions of mild thermal climatology (i.e. less thermal stress) whereas the hottest regions represent those areas that will experience the most extreme temperatures for a region (i.e. greater thermal stress). The final product was an accumulation of SST over a tidal cycle (one month). As represented, the blue regions portray those locations that likely experience greatest cooling at the surface due to mixing and hence represent the regions with the largest thermal capacitance. This provides the organisms that live there with a very mild climate, characterized by relatively small temperature ranges. In contrast, the red regions portray those locations that likely experience little to no mixing and hence represent the

least thermal capacitance. The organisms that live in these regions experience an extreme climate, characterized by relatively large temperature ranges.

A chart of this type is potentially extremely useful when designing a PAN. In general, most PANs are currently designed so as to provide protection to "representative bioregions", meaning that as much as possible, every type of bioregion within the ecosystem of interest should be equally represented within the PAN.

However, it is important to recognize that an ecosystem is not only made up of different species but also of organisms within each species that can have unique physiological characteristics. When designing a PAN, it is relatively straight forward to map bioregions on the basis of species composition, however the unique physiological characteristics within each species are not considered with these techniques. With respect to a changing climate, the unique physiological characteristics are likely to be grouped into regions that mimic the relative thermal ranges throughout the ecosystem. As a result, although we may not know what these characteristics are, the relevant characteristics for resilience against climate change are more likely to be better protected if representative samples of each thermal region within the thermal capacitance map are protected.

Table of Contents

Table of Figures

Table of Tables

Acknowledgements

There are many people who contributed to the success of this project. The field work had many helpers, so thanks go to: Debbie, Kyle and Luke McLean; the team at PICRC, in particular Steven Victor; Pat Colin and his team at the CRRF; David Hinchley, Andrew Smith and the rest of the Palau TNC team; and the many various departments of the Palau Federal and Koror State Governments. Thanks also to Bob Richmond from the University of Guam for loaning us a couple of current meters. Thanks to the NOAA/NOS team who worked very closely with us to produce the satellite derived bathymetry, and thanks to Joe Metzger from NRL for helping with the low frequency currents. Special thanks to Jessica Pejsa for her assistance in the administration of this project. Lastly, while NOAA and AIMS were the major source of funds for this project, this work could not have been undertaken without a significant injection of funds from the Michael and Andrea Banks Nature Fund via TNC.

Introduction

During the latter half of 1998, Palau experienced unprecedented bleaching that resulted in significant mortality and the loss of significant proportions of one of the few remaining pristine coral reefs in the World (Wilkinson, 2000). Prior to 1998 and since 1998, little to no coral bleaching has been observed. Figure 1 is a plot of accumulated heat stress for Palau, as measured by the National Oceanic and Atmospheric Administration (NOAA) Coral Reef Watch's Degree Heating Week (DHW) satellite product. A DHW value of 4 or more indicates significant bleaching (Liu *et al.*, 2003, Skirving, *et al.*, 2005). Note the DHW=4 line in Figure 1. The accumulated stress in 1998 easily surpassed that mark and is the only year to have done so since 1985. Note also that the heat stress for 1998 lies within the latter half of the year, as do most of the other small peaks.

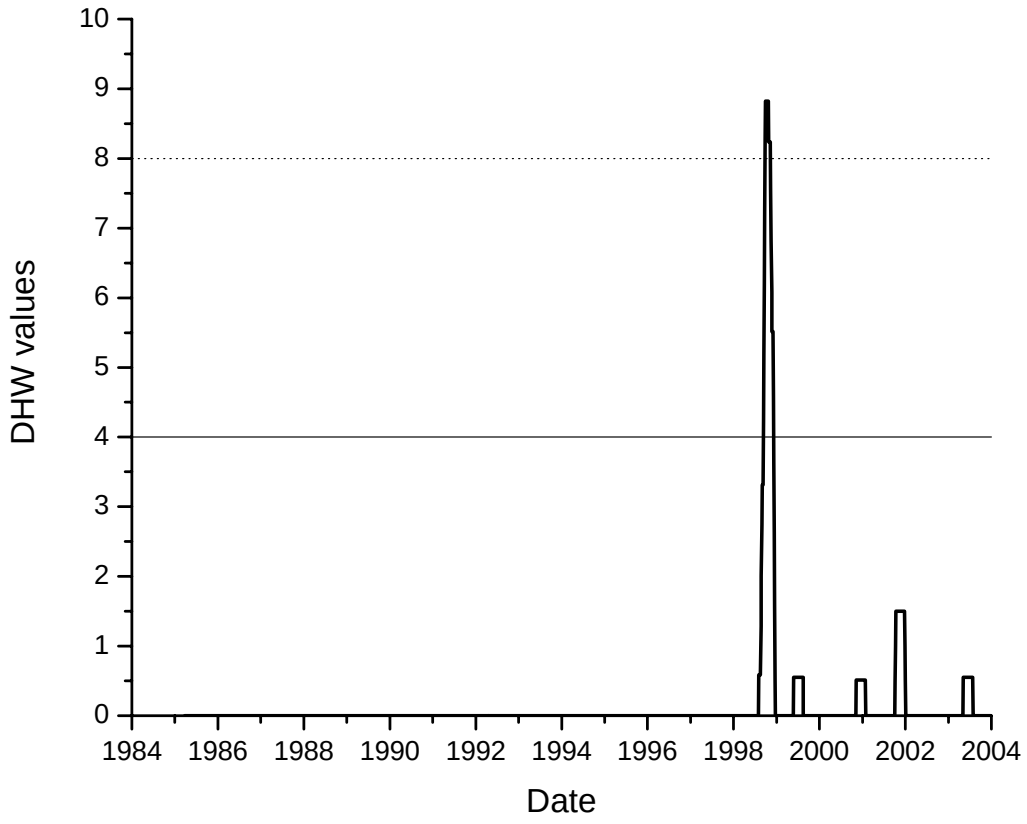

Figure 1 Accumulated thermal coral stress for Palau based on the Degree Heating Week (DHW) product for the period 1985 to 2004.

The Nature Conservancy (TNC) and the Palau Government have joined forces to assist in the design and implement a protected areas network (PAN) for Palau's coral reef ecosystem. Punctuated by the 1998 event, they recognized bleaching as one of the major future threats to the Palau coral reef ecosystem. With only one poorly documented

bleaching event to go by, it is difficult to gain enough information about the response of this ecosystem to this type of event to be able to build resilience to bleaching events into the PAN.

In parallel with the PAN, NOAA and the Australian Institute of Marine Science (AIMS) were collaborating on the development of the use of hydrodynamic models to predict heat stress during a bleaching event. In 2003, it was decided to combine these efforts and for NOAA and AIMS to produce a heat stress model for Palau for use in the PAN in an attempt to include resilience against changes to future climate.

This report is the final report for the NOAA/AIMS/TNC collaboration on the development of a model that describes spatial patterns of heat stress for Palau. It includes a description of the data collection, a description of the hydrodynamic model, and how this model was taken and used to derive patterns of heat stress for Palau.

Mass Coral Bleaching: Climate or Weather?

Mass Coral Bleaching

Coral bleaching is a generalized stress response by zooxanthellae and is not necessarily related to any one stressor (Glynn 1993). To date, mass coral bleaching events have been correlated with thermal stress (e.g., Dennis and Wicklund 1993, Drollet *et al.* 1994, Winter *et al.* 1998, Hoegh-Guldberg 1999, McField 1999, Berkelmans 2002). The physiological mechanism is that high temperatures damage the photosynthetic pathway, which leads to a breakdown of the photosynthetic process (Jones *et al.* 1998). After the thermal threshold is surpassed, the normally robust photo system can be overwhelmed by significant amounts of light, eventually causing the formation of reactive oxygen molecules that eventually destabilizes the relationship between corals and their symbionts (Hoegh-Guldberg 1999, Downs *et al.* 2002). Therefore, although light is an important factor in the coral bleaching story, it is not normally a stressor until water temperatures have exceeded certain limits (Berkelmans 2002).

Links between El Niño and Bleaching

There is much talk about El Niño being the "cause" of 1998. If this is so, we might expect to see a correlation between El Niño and bleaching around the world. Arzayus and Skirving (2004) took the NOAA Coral Reef Watch satellite-derived Degree Heating Week product (DHW) and using the suggested value of DHW = 4 to indicate bleaching, they hindcast bleaching back to 1985 for the entire world. They then took these hindcast bleaching events and compared them to the NCEP defined El Niño, La Niña and Neutral conditions (http://www.cpc.noaa.gov/products/analysis_monitoring/ensostuff/ensoyears.shtml). Using the rule that if 70% or more bleaching events occurred within one of these ENSO

states, then that 50km reef region is correlated, they found that only 0.2 % of reefs are correlated with an ENSO condition (0.05 % with El Niño, 0.14 % with La Niña, and 0.01 % with Neutral conditions).

Although they did not examine the effects of ENSO on bleaching severity, they clearly showed that the onset of bleaching is not correlated with ENSO for the vast majority of world reefs.

Bleaching weather

Given that the popular belief that ENSO is the cause of coral bleaching is incorrect, what is the cause? Skirving and Guinotte (2001) investigated the origin of the hot water that caused the Great Barrier Reef (GBR) to bleaching during 1998. They noted that a combination of low wind speed and neap tides was correlated with generally high sea surface temperatures (SST). They also noted that, during these periods of higher sea surface temperature, there were correlations between shallow bathymetry and locally-cooler SST and between deep water and locally-warmer SST.

These correlations led them to conclude that the hot water was a result of *in situ* heating from solar radiation, and that the effect of this heating was amplified by a lack of hydrodynamic mixing. The idea that SST anomalies leading to coral bleaching is mostly a result of *in situ* heating has since been supported by many field observations (Wilkinson, 1998 and 2000; Berkelmans *et al.*, 2004; Bird, *et al.*, 2004; Skirving *et al.*, 2004).

Very few mass coral bleaching events in the world are a result of advected hot water (Skirving, 2004). Little to no wind, clear sunny skies and weak ocean currents characterize these events and as such, *in situ* heating is the cause of almost all thermally-induced mass coral bleaching events. It would therefore be more accurate to describe mass coral bleaching as a weather phenomenon rather than the result of climate, as is currently popular. Climate is likely to modulate the frequency of these weather events, but more research is necessary before direct links between climate states (e.g., El Niño) and coral bleaching can be made.

Spatial Variability of SST During a Bleaching Event

Effects of Hydrodynamic Mixing

During a bleaching event, spatial patterns of SST are quite complex and have a scale of hundreds to tens of thousands of meters. Figure 2 is taken from Skirving and Guinotte (2001) and is an SST image of the southern Great Barrier Reef during the 1998 bleaching event. It clearly shows the high complexity that existed in the spatial patterns of SST during this event. Skirving and Guinotte (2001) also point out that this bleaching event

(like most others around the world) was characterized by bright sunny skies and very low winds. This is generally accepted as a crucial part of the formula for a thermally induced mass coral bleaching event.

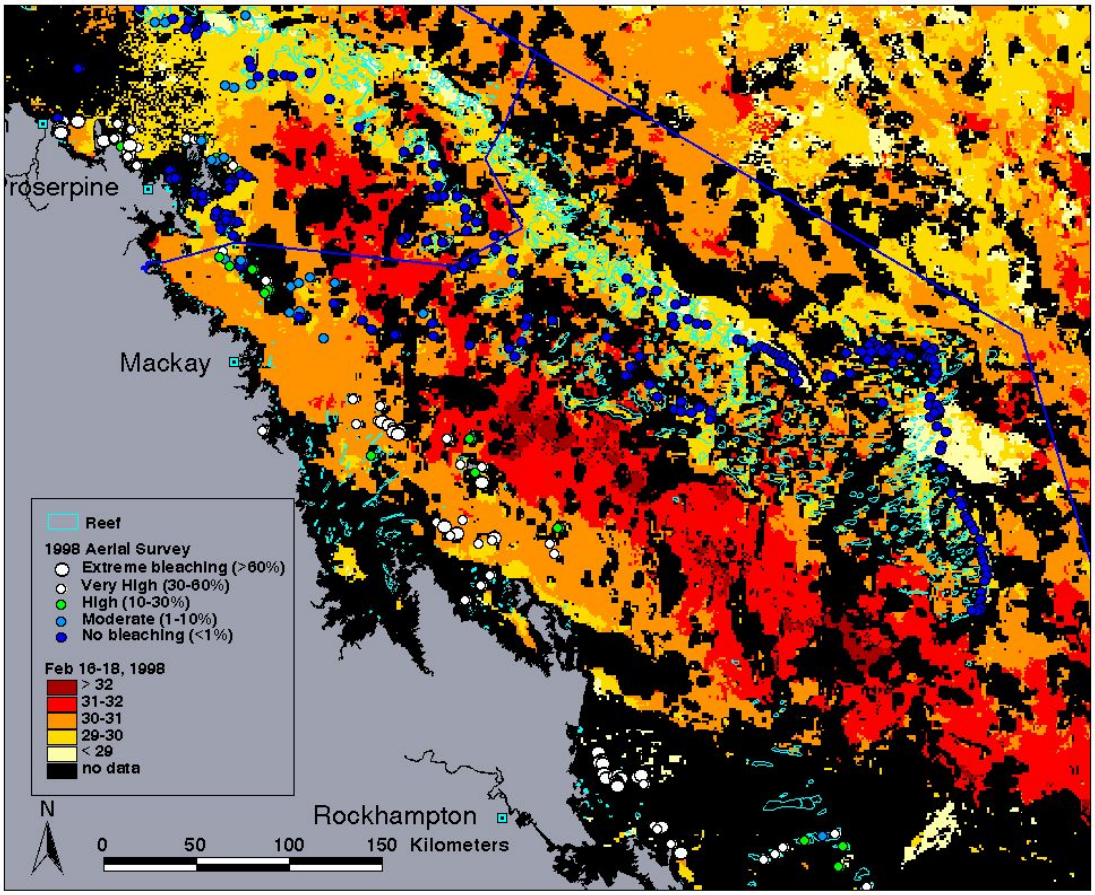

Figure 2 Average SST for 16-18th February for the Southern GBR region. Reefs and bleaching are also depicted. (from Skirving and Guinotte, 2001)

Given the existence of bright sunny skies (i.e. no cloud) and given that on these scales solar radiation is homogeneous in space, in the absence of wind, hydrodynamic mixing is the only mechanism that could create such a complex SST pattern (Skirving and Guinotte, 2001; Skirving, 2004; Skirving, *et al.*, 2004). Ninety eight percent of solar energy is absorbed within the top four meters of the surface of the sea. As warmer water is more buoyant than cooler water of the same salinity, during a bleaching event the warmer water will remain at the top of the water column unless there is a mechanical process to mix it down.

There are four different mechanisms that can vertically mix the water column; wind, low frequency currents (e.g., East Australian current, Gulf Steam, etc.), high frequency currents (e.g., tides) and swell waves. As described above, wind is not a factor for

hydrodynamic mixing during a coral bleaching event, so this only leaves swell waves and currents, which mix via bottom friction.

Since the water at the surface is warmer than the water below it, any vertical mixing will induce cooling at the surface and warming at depth. The deeper the mixing the cooler the surface will be. Therefore, during a bleaching event, there is a relationship between the patterns of SST and a combination of the depth of water and strength of the currents (Skirving *et al.*, 2004; Heron and Skirving, 2004).

Waves can also mix the water column, however during a bleaching event there is no wind so wind-waves are not a factor, but waves can be a factor where reefs are exposed to swell that is generated thousands of miles away.

The Physics of Ocean Heat Content and Distribution

During the daylight hours there is a net flow of heat into the ocean. The insolation flux is in the form of electromagnetic radiation which is absorbed in the upper layers of the ocean. The resulting warm layer may be mixed down by dynamical processes driven by currents and waves. The outflow of heat through the surface dominates at night. It is driven mainly by the temperature difference between the sea and the air, but there is a superposed effect of electromagnetic radiation. The combination of these fluxes gives a net diurnal variation whose long term average sets the climatological mean for the sea surface temperature. It is when the fluxes change that the temperature can vary significantly from the climatological mean and produce conditions of stress to the corals.

Specific physical processes affecting the flux and distribution of heat in the ocean are discussed here.

Insolation

Solar radiation is the primary source of ocean heat content. The solar radiation spectrum at the bottom of the atmosphere peaks in the visible range of wavelengths and has absorption lines and bands due to the composition of the atmosphere. The main control on the energy arriving at the sea surface is exerted by the aerosol and water vapour content of the atmosphere. As such, the type of air mass above a coral reef will have considerable influence over the amount of surface solar radiation. A clear sky with relatively low humidity and low aerosol content, such as can occur in regions such as the Red Sea and parts of the Great Barrier Reef, will provide maximum insolation. This is reflected in the extreme SSTs often recorded in these regions. Conversely, regions that experience dust storms, high humidity and cloudy conditions will experience lower amounts of insolation with the same sun angles, resulting in lower SSTs.

Absorption

The absorptive properties of the ocean water will define the depth-distribution of solar energy that is transferred directly to the water. A good model for the absorption of solar energy in the upper layer of the ocean is the exponential

$$I = I_0 \exp(-\alpha z) \tag{1}$$

where α is an absorption coefficient equal to the inverse of the e-folding depth, and z is the depth. Equation (1) works for a single absorbing constituent in the water, and for an absorption coefficient which has no variation with depth. This is often not the case. For example, if there is buoyant biomass then there will be an enhanced absorption layer near the surface; also, turbidity due to resuspension of benthic sediments is usually greater at the bottom of the water column, also enhancing absorption. Under these conditions the absorption has to be calculated by integration across layers of water. At the bottom of the i^{th} thin layer of thickness Δz the intensity is I_i where

$$I_i = I_{i-1}\left(1-\alpha_i(z_i)\Delta z\right) \tag{2}$$

The intensity of solar radiation at depth z_k is

$$I(z_k) = I_0 \prod_{i=1}^{k}\left(1-\alpha_i(z_i)\Delta z\right) \tag{3}$$

Typically, $\alpha \approx 0.5$ and the solar heating is effective in the upper 2 meters of the water column. If there is no mixing in the vertical water column then corals within the first two meters from the surface may be susceptible to heat stress and bleaching.

Dynamical Mixing by Currents

Vertical mixing of the water column alters the distribution of heat. Ocean currents have a tendency to induce mixing under most conditions. In shallow water, where coral reefs are most-often located, we can expect a boundary layer shear flow due to friction at the bottom of the water column. This is the basic response to ocean currents onto which we can superpose the effects of wind stress at the surface, stratification and wave-induced mixing. Note that the only concept of laminar flow is in the viscous layer at the bottom, and eddy diffusion prevails throughout the water column.

Mixing due to currents is driven by the vertical shear in the horizontal velocity of the water in the column and is carried out by eddies in the vertical plane. A commonly assumed model for the vertical eddy viscosity is the linear model given by

$$N_z = k u_* (H - z), \tag{7}$$

which leads to the logarithmic bottom-friction layer

$$u(z) = \frac{u_*}{k} \ln\left(\frac{H - z}{z_0}\right), \tag{8}$$

where z is the distance from the surface (positive downwards), H is the water depth, z_0 is the thickness of the viscous layer, u_* is the friction velocity and k is the von Karman constant. The vertical gradient in the horizontal flow has a shearing tendency which induces mixing.

Mixing of the vertical column due to bottom friction is strongest near the bottom where velocity shears are greatest. However with strong currents and shallow water this can impact on the mixing of the upper solar heated layer. One important thing about this simple theory of mixing in the logarithmic boundary layer is that it gives us a reference frame for thinking about turbulent mixing in the water column when velocity shears are caused by other phenomena.

Mixing due to Wind Stress

Vertical mixing of ocean waters can also be induced by winds. Wind at the surface of the sea produces momentum transfer to the water, and hence a wind stress velocity at the surface. The velocity at the surface is transferred down through the column by eddy diffusion. If we assume that the vertical eddy viscosity is controlled by the stress at the surface grows linearly with depth then we have a mathematical form similar to the bottom friction layer with

$$N_z' = k u_*' z \tag{9}$$

where z is the distance from the water surface (positive downwards), and u_*' is the stress velocity at the surface.

The actual eddy viscosity in the water column is a combination of N_z' and N_z; the velocity profile is a combination of the bottom boundary layer and the surface boundary layer. This leads to complications in numerical modeling of the currents and various schemes have been suggested for combining the eddy viscosity terms.

It is clear that the velocity shears induced by wind at the surface of the water have a significant role in the vertical mixing of the surface solar heated layer.

Mixing due to Wave Breaking

Ocean waters can also be vertically mixed by breaking waves. In the open ocean, most of the wave energy is conserved and not lost to mixing processes. It is only when the waves become non-linear that they lose energy to turbulence. It is the process of wave breaking that dominates the transfer of wave energy to mixing. At reef fronts the transfer is almost complete with only a remnant of wave energy being reflected back to the ocean, some of it transferring to a forward bore in the breaking wave, and a significant fraction going into turbulence at the breaker location. For a propagating surface gravity wave most of the energy is in the upper part of the water column. This is illustrated in Figure 3 where we show the depth profile of the horizontal surge velocity for a wave with 1 m amplitude (trough to crest) and 6 s period. This is a typical oceanic wind wave and the graph shows how the velocity decreases rapidly with depth. If there is any non-linearity or breaking then the associated energy becomes available for mixing.

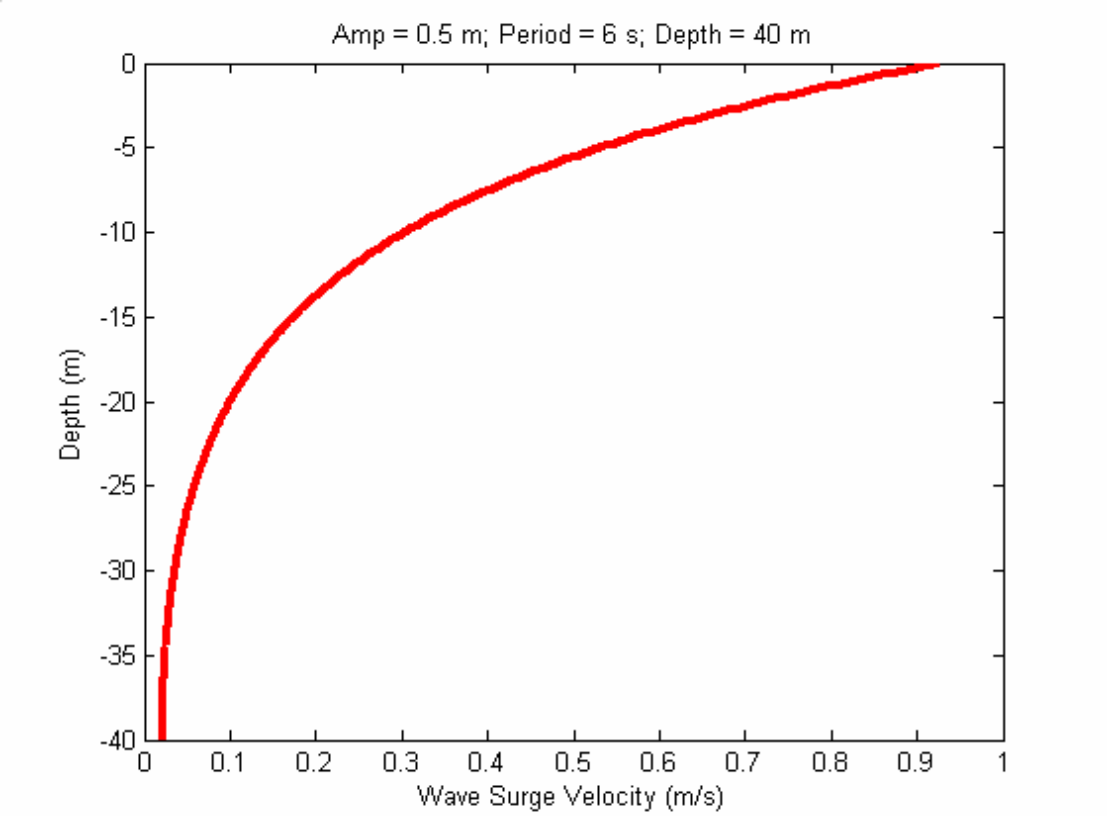

Figure 3 Horizontal surge velocity versus depth for a typical wind wave. Most of the wave energy is in the top few meters. The vertical surge velocity profile follows the same curve near the surface but departs and goes to zero at the bottom of the water column, set to 40 m here.

The kinetic energy density for a wave with amplitude a, angular frequency ω and water depth d is given by

$$KE(z) = \frac{1}{2}\rho\left(u^2 + w^2\right) \tag{10}$$

where u, and w are the horizontal and vertical depth-dependent particle velocities averaged over one cycle:

$$u^2 = \frac{\pi a^2 g^2 k^2}{\omega^2}\frac{\cosh^2\left(k\left(d+z\right)\right)}{\cosh^2\left(kd\right)} \tag{11}$$

$$w^2 = \frac{\pi a^2 g^2 k^2}{\omega^2}\frac{\sinh^2\left(k\left(d+z\right)\right)}{\cosh^2\left(kd\right)} \tag{12}$$

This wave energy is generally not available for mixing on shelf waters. However, when a wave encounters a reef front it loses most of its energy and provides a dominant mixing effect for the solar heated layer near the surface. This effect is so dominant that it is difficult to think there would be coral bleaching on the weather side of a reef except in very flat-calm conditions. Waves breaking on the reef front also send pulses of water forward across the reef flat. This pulsing bore is also well-mixed and we would expect mitigation of bleaching on the parts of the reef flat that are flushed with this water.

The physical processes of wave breaking on the reef front and the subsequent pulsing of water across the reef flat have a strong mitigating effect on coral bleaching.

Stratification of Ocean Water

Horizontal stratification imposes an impediment to mixing, and therefore heat transfer, due to the potential energy of the stratification. The Richardson number compares the energy of stratification and the turbulent kinetic energy and provides us with an index to measure the severity of the stratification.

Under high Richardson number conditions there is likely to be a strong vertical shear at the boundary between the stratified layers and the turbulent kinetic energy works to erode the stratified layer.

Following the approach of Simpson and Hunter (1974), de Silva Samarasinghe (1989) and others, we consider the rate of loss of potential energy to be equal to some small fraction per second, σ, of the turbulent kinetic energy as

$$\frac{\partial}{\partial t}\left(PE\right) = -\sigma\left(KE\right), \tag{13}$$

which can be written as

$$\frac{\partial}{\partial t}\left\{\int_0^h gz\left(\rho-\bar{\rho}\right)dz\right\}+\sigma\bar{\rho}\int_0^h N_z\left(\frac{\partial u}{\partial z}\right)^2 dz=0\,, \qquad (14)$$

per unit area of the water column, where h is the water depth, $\bar{\rho}$ is the mean water density in the column at depth $\bar{h}$, and N_z is the vertical eddy viscosity. Simpson and Hunter (1974) found $\sigma = 0.0037\ s^{-1}$ in the Irish Sea; Hearn (1985) derived a similar value.

Stratification is an important phenomenon for coral bleaching. When the sun heats the surface layer, the density of that layer is reduced and there is an inherent stability caused by the density stratification which is conducive to coral bleaching. Current shears are likely to be enhanced at the boundary between stratified layers and equations (13) and (14) become important in estimating the impact of the solar heating. If there is wind stress driving currents in the warm surface layer then there is likely to be an enhanced mixing at the boundary of the stratification. Thus, the formation of stratification by solar heating of the upper layer is conducive to coral bleaching, but it can also set up strong current shear zones which can assist mixing. The effects of solar heating and turbulent mixing are finely balanced here.

Another form of stratification is the thin surface layer which is evaporatively cooled by water vapour flux from the ocean to the atmosphere. This is a thin layer of the order of millimeters, with a regeneration time constant of several seconds if it is destroyed, for example by a micro-breaker. This layer is unstable in the water column and promotes mixing. When we put this micro-layer mixing in the context of solar insolation on the order of a meter depth below the surface it is quickly lost in the scales of energy transfer and penetration depth. A more significant effect of the "skin layer" is that it is this layer which provides the infrared radiation used by satellite radiometers to measure the surface temperature. The skin layer reduces the brightness temperature by up to about half a degree (perhaps more in tropical waters). This is not a random error, but is a variable offset in the measured temperature which depends on the nature of the skin layer.

The skin layer has little impact on coral bleaching because it is so thin that it does not contain much heat energy.

Hydrodynamic Modeling for a Bleaching Event

As each of the physical processes discussed above influences the transfer of heat into and within the water column, they can thus affect the potential for coral bleaching to occur. As mentioned previously, winds are effectively absent during a mass bleaching event, which leaves swell waves and currents as the only mechanisms capable of altering the spatial patterns of SST. Swell waves are very effective mixers where they exist and can mix the water when they impinge on a reef. However, they are not capable of cooling an entire reef and will not be available for every reef since not all reefs are exposed to swell waves and not all bleaching events have swell.

This leaves currents as the only reliable mechanism for altering spatial patterns of SST. The vertical temperature profile is determined by heating from above via incoming solar radiation and cooling from below via upwelling, breaking internal waves and cold-water intrusions. Currents then mix this vertical profile via bottom friction and 3D mixing behind reefs and islands. Advection can be a horizontal mixing mechanism associated with these currents in some situations. The spatial pattern of mixing interacts with the spatial pattern of vertical temperature profiles to create patterns of low to high SST during a bleaching event.

Constructing a Model for Palau

In parallel with the PAN, NOAA and AIMS were collaborating on the development of the use of hydrodynamic models to predict heat stress during a bleaching event. In 2003, it was decided to combine these efforts and for NOAA and AIMS to produce a heat stress model for Palau for use in the PAN in an attempt to build in resilience against future climate change.

For the model to be constructed, NOAA and AIMS needed:

a. Calibration and Validation Data for the model: Due to a dearth of hydrodynamic data for the Palau region, all data needed to be collected by this project.
b. The Palau bathymetry: Due to a lack of available data, NOAA derived the bathymetry from a combination of Landsat data and bathymetry transects taken with a depth sounder from a small boat. This produced a chart with 250 meter horizontal resolution and an rms precision of 1 meter vertically.
c. Low frequency currents: A combination of the Navy Research Laboratory's (NRL) Navy Layered Ocean Model (NLOM) and NOAA's Ocean Surface Current Analyses – Real time (OSCAR) were used to derive the seasonal low frequency currents around Palau.
d. High frequency currents: A combination of tide gauge data collected in and around Palau was used to derive a model that could accurately predict the tides. The bathymetry and the tidal model were then used with the Princeton Ocean Model (POM) to build a model of tidally induced currents in and around Palau. Field data collected over a period of 5 months were used to calibrate and validate the output of this model.
e. Vertical temperature profile: This was derived by modelling a patch of water with a homogeneous temperature and applying a diurnal cycle of solar radiation for a period of two weeks.

Hydrodynamic data collection

An extensive study of oceanographic parameters in Palauan waters was undertaken during the period August 2003 – January 2004. The timing of the deployment was selected to coincide with the time of year during which bleaching events have been observed. Sixty-two instruments were deployed in and near the Palau lagoon to record currents, temperatures, sea-levels, salinities and weather conditions. This number of instruments is unusually high for a region of this size; the largess of the deployment was fueled by a desire to maximize coverage and the fortuitous availability of instruments. The deployment is the most-extensive *in situ* ocean study ever performed in Palau. The data have been made freely available and are described in the Palau Oceanographic Array Data Report which is attached here as Appendix 1.

For the purpose of the broader project, i.e., to study SST patterns leading to coral heat stress, the Palau lagoon was partitioned into three study areas; the Lagoon box, the Malakal Harbour box and the Rock Islands box. The extent of the Lagoon box, illustrated by the orange line in Figure 4 was primarily described by environmental boundaries (island or reef barriers). This suggests that the majority of water movement in and out of the box is through the channels at the boundaries. Hydrodynamic models of the lagoon circulation can be constrained at the boundaries by the measured flow through these channels. Current-measuring instruments were placed in the major channels; sea-level monitors were deployed on reef flats and across the box; salinity meters were placed in an east-west transect across the lagoon; and temperature sensors were positioned in vertical profiles throughout the box (for details, see Appendix 1).

The Malakal Harbour and Rock Islands boxes were defined as sub-regions of the Lagoon box, as shown in Figure 4. These regions, like the Lagoon box, are bounded by islands and/or reefs, again providing a sensible boundary for hydrodynamic models. These regions are of particular interest for economic, environmental and scientific purposes. Instruments were deployed at the boundaries of and within each of these boxes. As for the Lagoon box, instruments were placed at boundary locations of major water movement. Data from these will aid in future modeling efforts for these regions. Detailed maps of individual instrument deployments are provided in Appendix 1.

All but one of the instruments, a temperature logger, were recovered. Two of the instruments recorded data intermittently and one recorded no data due to power supply difficulties. Despite these setbacks, the dataset from the recovered instruments provides a broad description of Palauan waters and proved to be invaluable during the modeling phase of this project.

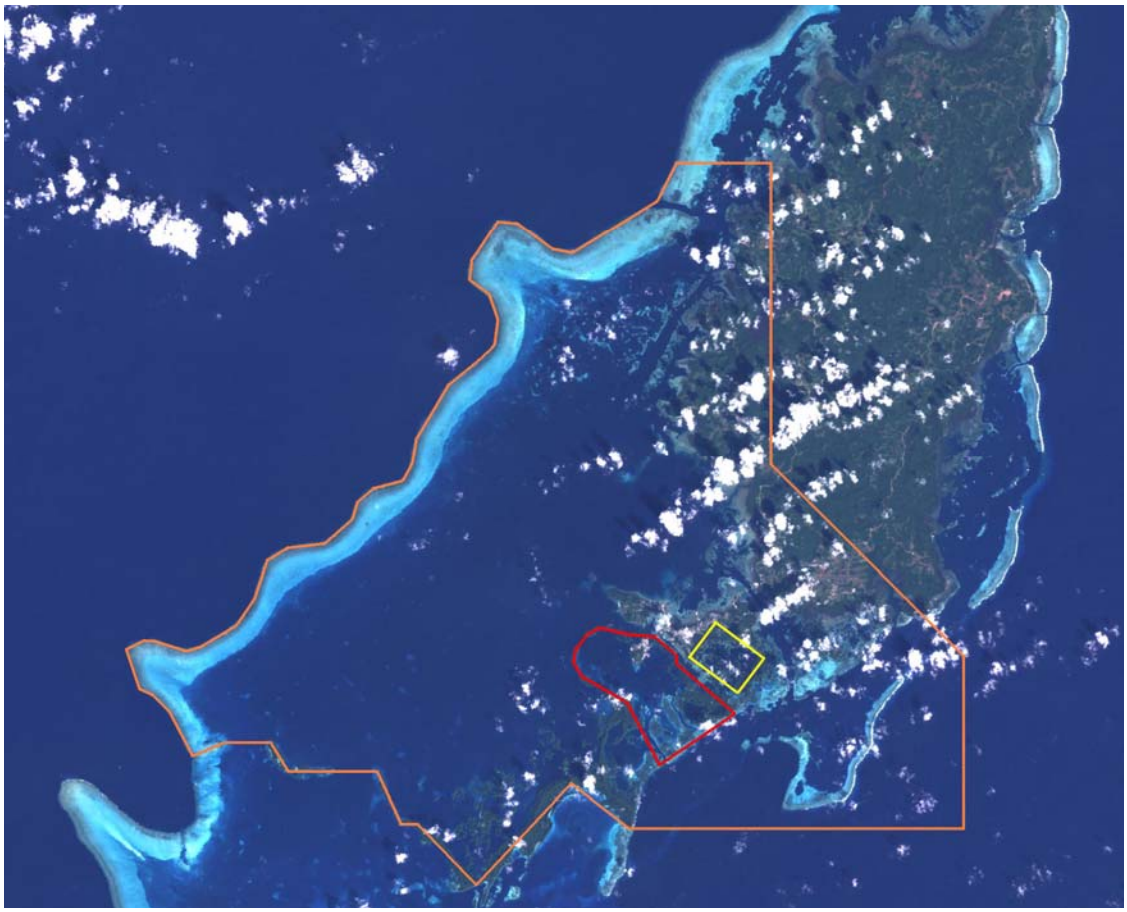

Figure 4 Landsat image of Palau showing the Lagoon box (orange), Malakal Harbour box (red) and the Rock Islands box (yellow).

The Hydrodynamic Model

The hydrodynamic model was designed specifically to produce a map of accumulated heat stress for Palau. However, the output may also be useful for other applications; e.g., particle tracking and connectivity modeling. The model code, commonly known as the Princeton Ocean Model (POM) (described in Blumberg and Mellor, 1987), was employed for this study. POM is a terrain-following (σ-coordinate) model with a staggered horizontal finite-difference scheme (Arakawa C-grid). A rectilinear horizontal grid was selected for the Palau model.

For the heat-stress map, the desired output from the hydrodynamic model is a two-dimensional map of time-varying currents. To achieve this, a suite of initial- and boundary-conditions was required to drive the model calculations. As the region of interest for Palau consists entirely of islands surrounded by open ocean, the extremities of the model domain were "open" – i.e., there were no land boundaries. Open boundaries require the definition of parameters to constrain the flow. Most numerical model

applications have at least one or two "closed" boundaries; this simplifies the model setup and also aids in accurately constraining the model output. Four open boundaries presented a challenge to the modeling process and increased the importance of precision in defining the constraints. The processes of some of these; determining model bathymetry, investigating low-frequency circulation in the region and modeling of tidal variations; are described in detail below.

Bathymetry

An accurate description of bathymetry is paramount for the success of a hydrodynamic model. The desired horizontal resolution for the model of Palau was around 250 m so as to resolve many of the topographic features of the region while maintaining sufficient computational efficiency.

Nautical charts of Palau, produced by the U.S. Defense Mapping Agency, were acquired to reference depth data. These charts were primarily based on data from World War II era Japanese surveys and a 1969 U.S. survey. By virtue of the navigational purpose of the charts, the values stated are lowest-tide values and err towards underestimation. While they are able to provide a general shape for the Palau lagoon, the data were neither accurate enough, nor of sufficient spatial consistency, required for the model. In addition, some feature details may have changed during the 35 years since the most-recent survey.

Further bathymetric information for the Palau lagoon was derived from Landsat imagery. These data were produced by the Special Projects Office of NOAA's National Ocean Service. The process used to derive estimated depth for Palau is described in Newhall and Rohmann (2003) following the technique of Stumpf *et al.* (2003). The accuracy of the estimated-depth algorithm is to within 1 m and the depth limit is 20-25 m (R. Newhall, *pers. comm.*). The Landsat images were geo-rectified and mosaicked using the Universal Transverse Mercator (UTM) grid system. The image data were transformed to estimated depths by comparing the ratios of the satellite spectral channels. The bathymetry values were calibrated using *in situ* data and observations of benthic habitat types. Bathymetry data were collected within the Palau lagoon using a dual-frequency depth sounder, mounted on a 21-foot vessel, along transects totaling more than 300 nautical miles. The spatial resolution of Landsat imagery is 28.5 m; averaging across 9×9 pixels provided the desired resolution for input to the model (256.5 m). Land boundaries were checked and corrected manually especially in locations with narrow channels that are important to the water exchange, e.g., the Rock Islands. A significant portion of the lagoon was too deep for the satellite algorithm and, as such, a deepwater dataset was required to augment the bathymetry.

Large-scale bathymetric data were acquired from several databases. Following the recommendation by Marks and Smith (submitted to Marine Geophysical Researches), the data of Smith and Sandwell (1997) were selected for the region surrounding Palau. The depths are derived from satellite gravity data combined with ship measurements and have resolution of two-arc-minutes (approximately 3.7km near the equator). The dataset were

re-gridded to the UTM grid and interpolated in two-dimensions at the Landsat gridpoints. The Smith & Sandwell interpolated data were then patched into the Landsat data where the Landsat depths were greater than 20 m. The combination of the two datasets introduced some erroneous values where the datasets were joined. These values were checked and corrected manually, as were discontinuities and spikes in the combined data.

Following these refinements, there were three areas for which the bathymetry appeared to vary greatly from the navigational charts; in the western section of Kossol Passage, to the north of Ulong Island and the region immediately north of Peliliu. The first and second of these appeared to be due to loss of vertical resolution during the interpolation of the deep-water data. Faulty values were removed from the data and, where available, *in situ* measurements and navigational chart readings were inserted. The remaining vacant gridpoints were assigned depths by kriging the existing data, a process involving statistical interpolation of the data. The error to the north of Peliliu was due to an incorrect land-mask in the Landsat data. The waters of this region are shallow and the bottom surface type is either white sand or near-black seagrass. Incorrect parameterization of the bottom type causes the depth algorithm to revert to land or deepwater, respectively, for these cases. The bathymetric data were corrected manually using *in situ* measurements and chart readings. The final dataset has horizontal resolution of 256.5 m and is the most-accurate, wide-scale bathymetry of Palau in existence. Figure 5 (a) and (b) illustrates the bathymetry.

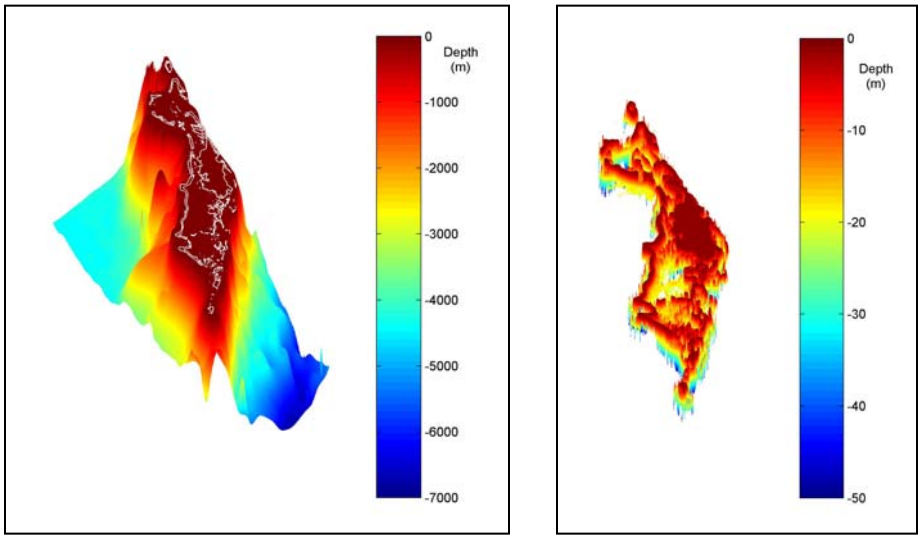

Figure 5 (a) Final bathymetry dataset for model domain. The white contour shows the land and barrier reef boundaries. (b) Bathymetry data to a depth of 50 m, showing lagoon features.

Low-Frequency Circulation

With bathymetry defined across the model domain, temporally-varying boundary conditions for the model were investigated. The first study was to determine low-

frequency currents in the region, i.e., currents varying on long time-scales. Examples of these types of currents around the world include the Kuroshio, the Gulf Stream and the East Australian Current. A literature search was undertaken for previous studies of the circulation in the immediate vicinity of Palau; no such studies were found. Due to this lack of prior information, it was necessary to include in this project a study to determine the existence of a seasonal variation in the surface currents in the western equatorial Pacific. The geographical area investigated is shown by the dotted line in Figure 6(a). A manuscript (Heron *et al., submitted*) discussing the results of this study has been submitted to the Journal of Oceanography; the submitted version is included in this document as Appendix 2. The results are summarized below; see the appendix for further details and literature references.

Previous work in this region focused on the major currents displayed in Figure 6(b); the North Equatorial Current (NEC), the Mindanao Current (MC), the Kuroshio, the North Equatorial Counter-Current (NECC) and the Indonesian Through-Flow (ITF). Further studies investigated two major mesoscale eddies in the region; the Mindanao Eddy (ME) and Halmahera Eddy (HE), also shown in Figure 6(b). These studies reported the high- and low-frequency variability of these features but none investigated annual patterns of the flow further to the east, near Palau.

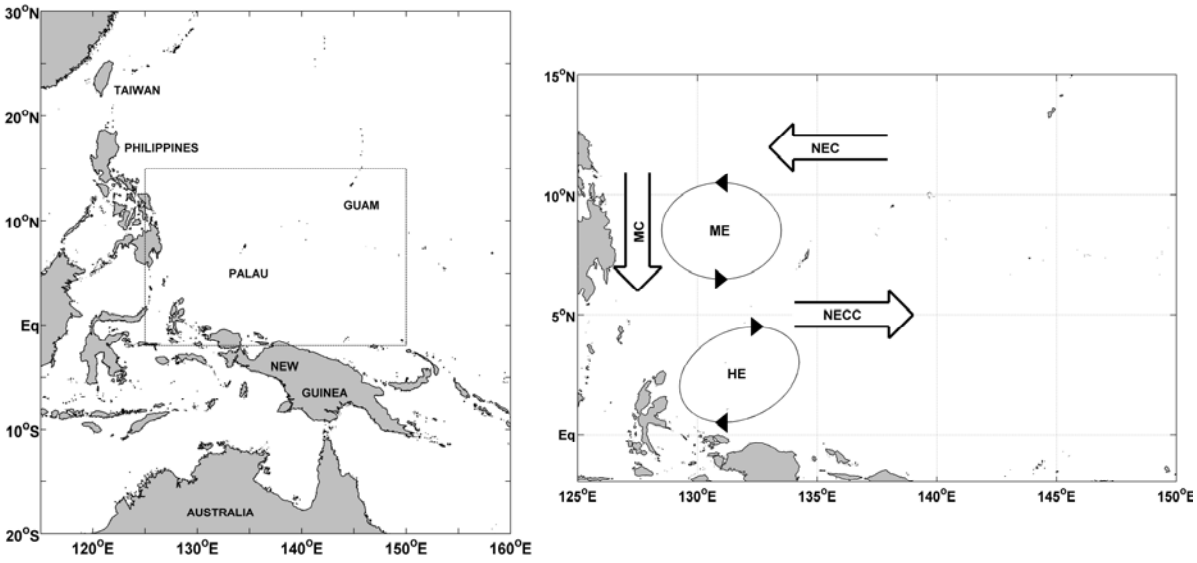

Figure 6 (a) Map of the western equatorial Pacific Ocean. The dotted line indicates the region considered in the study by Heron *et al.* (*submitted*). (b) Schematic representation of the surface features reported in literature.

Data from the Ocean Surface Currents Analysis – Real-time (OSCAR), TRIangle Trans-Ocean buoy Network (TRITON), the Joint Archive for Shipboard Acoustic Doppler Current Profiler (JASADCP); and output from the Naval Research Laboratory Layered Ocean Model (NLOM) and were examined and compared. Monthly climatologies of the surface currents from the OSCAR and NLOM datasets were examined for seasonal

variations. The JASADCP data were used to validate the NLOM output. The timing of the observed seasonality in the surface currents around Palau was consistent with the annual variation in the surface winds from the TRITON data. The existence and variability of documented surface features, previously mentioned, was verified and additional features were identified in the study region. These are shown in Figure 7 and were named the Palau Eddy (PE), Caroline Eddy (CE), the Micronesia Eddy (MiE) and the Papua New Guinea Eddies (PNGE) – a family of eddies along the north coast of New Guinea. The seasonal variation of the NECC Tail, i.e., the section east of 135°E, was also determined and discussed.

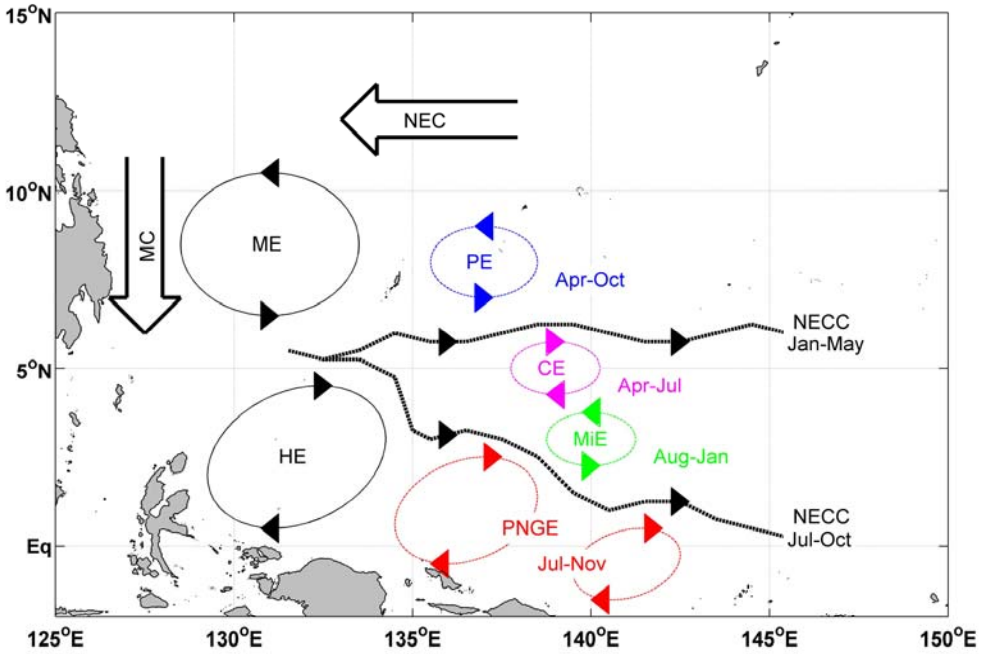

Figure 7 Surface features described by Heron *et al.* (*submitted*). Newly described features may be identified by comparison with Figure 6(b).

Low-frequency currents near Palau are driven by the major surface features; the seasonal variability of the currents follows that of the major features. North of Palau, the NEC varies only slightly in both magnitude and direction. To the south, the NECC Tail migrates seasonally and varies in magnitude; this significantly affects the fluid motion around Palau. The ME and HE are present throughout the year and vary seasonally in both extent and location. The PE exists from April to October and influences the flow to the east of Palau during this period. Figure 8 is a schematic diagram of the annual variation in the surface currents surrounding Palau. Heron *et al.* (*submitted*) note that the low-frequency currents are weak and disordered from July to September. This is consistent with the timing of observations of coral bleaching events. The observed surface currents, as described by Heron *et al.* (*submitted*) were employed as the velocity boundary conditions for the hydrodynamic model.

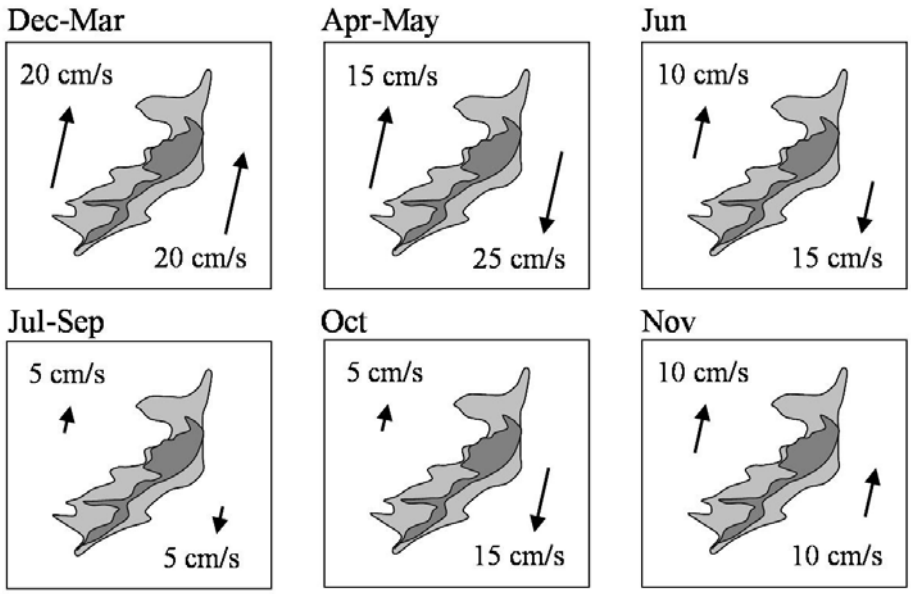

Figure 8 Schematic diagram of the seasonal variation in the currents around Palau.

Tidal Elevation

Variation in the sea-surface elevation is required as input for the numerical model. The boundaries of the model domain are located in deep-water sites where little or no tidal data have been recorded. While the determination and use of tidal constituent vectors would be preferred to constrain the tidal variation, this was near-impossible for the this study, due to a lack of existing data. A sensible and suitable proxy to determine the effects of tides is to constrain values using a sea-surface elevation time-series. Again the remote location of the domain boundaries is an issue; however, in this case the extended time-series of sea-level from the Malakal Harbour Tide Gauge may be employed. This tide gauge dataset is the only extended time-series in the vicinity of Palau.

A near-continuous dataset of hourly elevations at Malakal from 1969-2004, as well as 15-minute-interval data for 1990-2001, were acquired from the Global Sea Level Observing System (GLOSS) [http://www.bodc.ac.uk/services/glosshb/stations/gloss120.htm]. The long-term average sea-level was determined from the data and defined as the datum for use in the model (i.e., the average was set to be zero). The time-series for Malakal was adapted and used for the boundary condition for elevation, phased across the model domain from east to west. This assumed that every elevation along the eastern boundary was in-phase, similarly with the western boundary. The assumption here was based on the tidal charts of Luther and Wunsch (1975) and on a global tide model by the University of Texas' Center for Space Research [animated at http://geodesy.eng.ohio-state.edu/tide.html]. The phase of the tidal signal was interpolated across the north and south boundaries throughout the model run. The adaptation of the Malakal elevation values for the boundaries was defined so as to closely replicate the observations at the tide gauge location. Several iterations of the model were required to determine the appropriate linear relationship. This process is discussed further below.

The elevation input was from 1200 hours, 28 October 2003 for a period of thirty days. This was chosen so that the model would coincide with the majority of data collected (see Appendix 1) and to encompass a lunar month (29.5 days) , the period through which the Moon returns, in phase, over a particular location on Earth.

Other Defined Parameters

Bleaching Weather (described above) is characterized by little-or-no wind. Applying a no-wind constraint in the hydrodynamic model is therefore valid and will simplify the model.

Bottom friction will vary with benthic habitat type; e.g., coral cover would have a greater drag than sand. A coefficient of bottom friction is defined for each gridpoint and is a logarithmic function involving the local depth, Von Karman's constant (0.4) and a roughness length. The latter of these was varied to represent difference in friction for different bottom types. Observations of the Palau lagoon showed that many shallow regions were covered by coral, while the major channels were covered by silt. To automate the definition while effectively capturing this contrast, the roughness length values were defined as a function of the water depth; shallow regions having greater roughness length than deep regions. While some coral-covered regions are in deep water, this method is effective and efficient in automating the characterization of bottom friction.

Output

The hydrodynamic model was run for thirty days including one-half day of spin-up time (to allow the solution to converge smoothly from the initial conditions). This length of simulation was defined to include a lunar month (29.5 days). The tide data are shown in Figure 9 with heights referenced to the long-term mean of the data. The period covers two spring tides (11 and 26 November) and two neap tides (03 and 18 November).

Software used in the post-processing of the model output, i.e., the production of the heat-stress map, constrained the duration of individual model runs to 1.5 days. Each subsequent 1.5-day run was continued from the final conditions of the previous run.

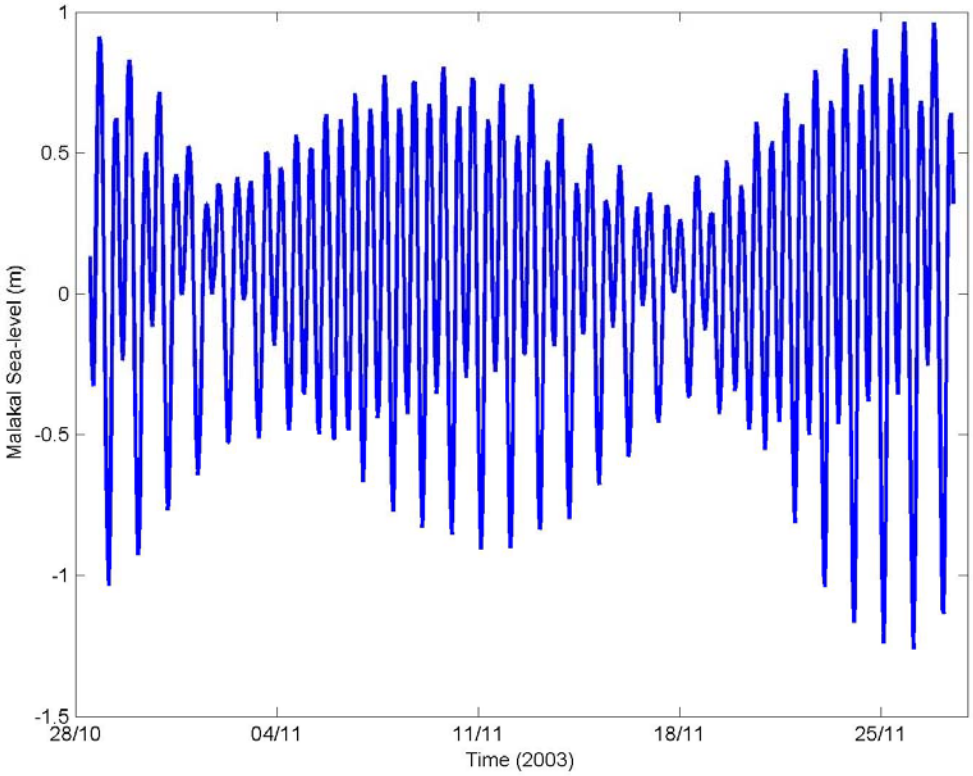

Figure 9 Time-series of sea-level measurements in Malakal Harbour used in the hydrodynamic model. The datum is the mean of measurements for the period 1985-2004.

As stated previously, the elevation boundary conditions were defined as a function of the Malakal Harbour Tide Gauge data. The linear relation at the eastern boundary was determined by iterative comparison of the data with elevations from the co-located grid point. There is a time lag in the tidal elevation between the eastern extent of the model domain and the tide gauge location. To determine this time lag, correlation coefficients of the elevations from these locations were calculated with varying time separations. Table 1 shows the correlation coefficients for each time-lag step. As the temporal resolution of the model output is one hour, this constrains the resolution with which the time-lag of the sea-level can be defined. From the correlation values in Table 1 it can be seen that the time-lag from the eastern boundary to Malakal Harbour is between two and three hours – and closer to two hours. Figure 10 shows a comparison of the model output at the tide gauge gridpoint with the measured sea-levels used to define the eastern boundary condition, with a two-hour time shift of these values. The results are for the entire simulation. A linear regression of the values gave a slope of 1.04 and intercept of 0.06 m. Figure 10 also shows the line of equity (i.e., the 45° line) for reference. From this analysis it can be seen that the method of defining the elevation boundary conditions has been successful.

Time Lag (hours)	Correlation Coefficient
0	0.51559
1	0.83044
2	0.97640
3	0.92102
4	0.68110
5	0.31699
6	-0.08324

Table 1 Correlations between the elevations at the Malakal Harbour Tide Gauge grid point and the eastern boundary grid point for varying time lags. The Malakal grid point lags behind the boundary grid point in each case.

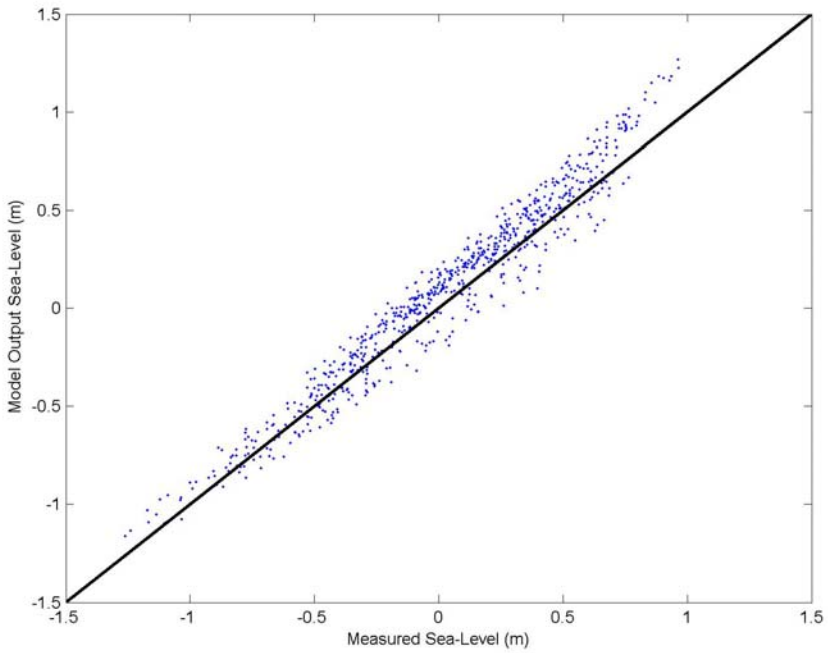

Figure 10 Scatter-plot of Malakal Tide Gauge sea-level values, model output versus measured values, for a two-hour time lag in the Malakal output from the eastern boundary. The solid line is at 45°.

The described seasonal variation in the velocity boundary condition was also applied in the model. Examination of output using different velocity constraints showed that the currents inside the Palau lagoon showed negligible variation from season to season, i.e., the lagoon currents are tidally-dominated. For this reason, results from the thirty-day run

for only one velocity boundary condition are presented, corresponding to the period July-September. This is, historically-speaking, the hottest period of the year and shows the greatest potential for coral bleaching (Bruno *et al.*, 2001).

Output from the Palau hydrodynamic model is illustrated in Figure 11 and Figure 12, showing currents vectors and sea-level, respectively, at the first time-step after the spin-up period (model time 0.5 days). Animation files of the model output are provided in the attached CDROM as "PalauModel_Velocity.avi" (vel_movie) and "PalauModel_Elevation.avi" (elev_movie), respectively. The movies have a time-step of one hour, matching the output frequency of the model. For presentation purposes, the resolution of the vectors shown in Figure 12 is 1/27th of the actual grid resolution (i.e., the spacing between arrow-tails is approximately 7 km).

In vel_movie the variation through the tidal cycle is reflected in the relative magnitudes of currents vectors through time. The strongest currents occur in the channels at the edges of, and within, the Palau lagoon (see also Figure 11). Notice the low magnitude of currents in the northern lagoon (the "Lagoon box" in Figure 4), while the southern lagoon (south of Ulong) has much stronger currents. The currents outside the Palau lagoon are generally stronger than those inside. Neap tidal periods coincide with the lowest-magnitude currents and spring tides with the highest currents, as expected.

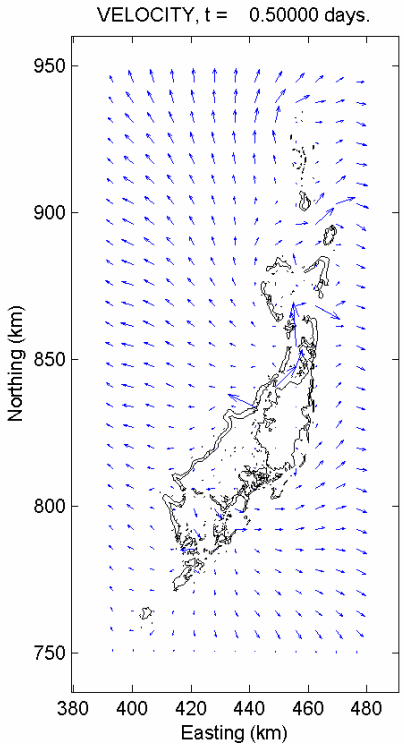

Figure 11 Surface velocity vectors at model time 0.5 days. Vectors are plotted at 1/27th of the grid resolution.

In elev_movie the tidal variation is apparent, as is the phase lag of the lagoon sea-level compared with the deep-ocean water. There appears a slight phase-difference between the northern- and southern-lagoons, which can also be seen in Figure 12. This is consistent with field observations for the region (C. McLean, pers.comm.). The variation in sea-level through the neap and spring periods of the tidal cycle is also evident in the animation.

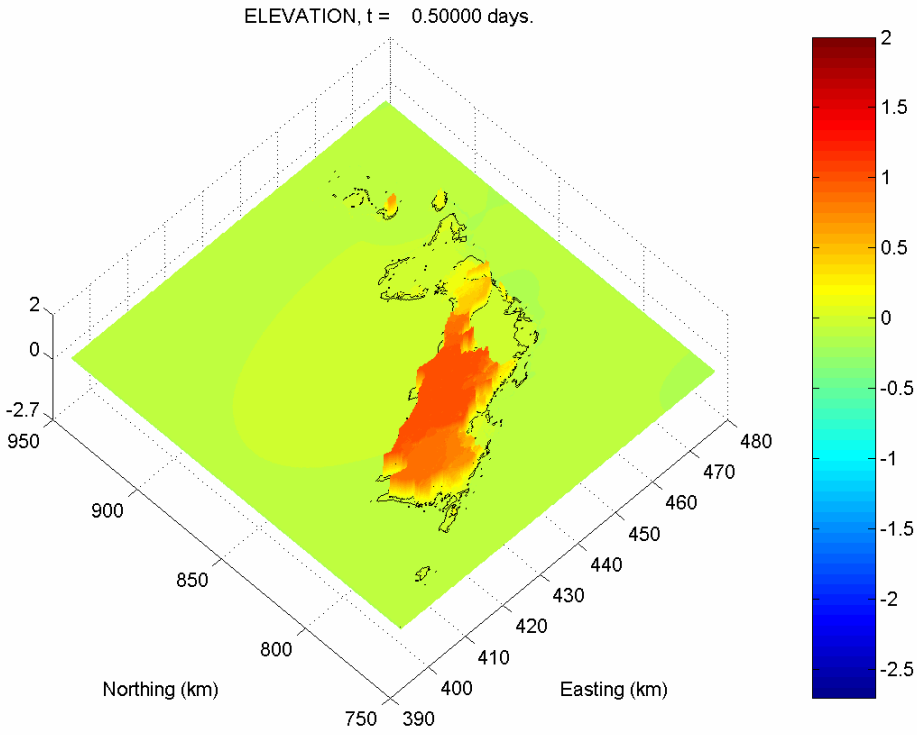

Figure 12 Sea-surface height, referenced to the long-term mean sea-level, at model time 0.5 days. The vertical axis and colour scale have units of meters.

While qualitative analyses of the model output suggest that it has been successful in describing the hydrodynamics of the region, further quantitative investigation is necessary to confirm the skill of the model. This was achieved by comparing data acquired during the deployment with output from corresponding model gridpoints.

The horizontal resolution of the numerical grid (256.5 m) was greater than the width of some channels in the Palau Lagoon. One of the defining parameters of POM is to conserve mass. As such, for a given rate of mass flow, a wide channel should have a speed of lesser magnitude as compared with a narrow channel. This effect was accounted for when comparing the model output with the data. Actual channel widths were determined using the 28.5 m-resolution Landsat bathymetry data and used to compare the volume flow rates between the model and data.

Figure 13 shows a plot of data (blue line) and model output (red cross) for the Lighthouse Channel (Toachel Ra Kesebekuu - instrument A8) from the first 1.5-day model run (including 0.5 day spin-up time). The data from the current profiler located in this channel were averaged in the vertical direction, so as to compare with the (vertical-average) output of the 2-D model. In Figure 13 the model output current magnitudes are scaled by the ratio of the actual to modeled channel-widths for comparison with data values. The upper panel of Figure 13 shows the magnitudes for the scaled model output and data; the lower panel shows the directions of each.

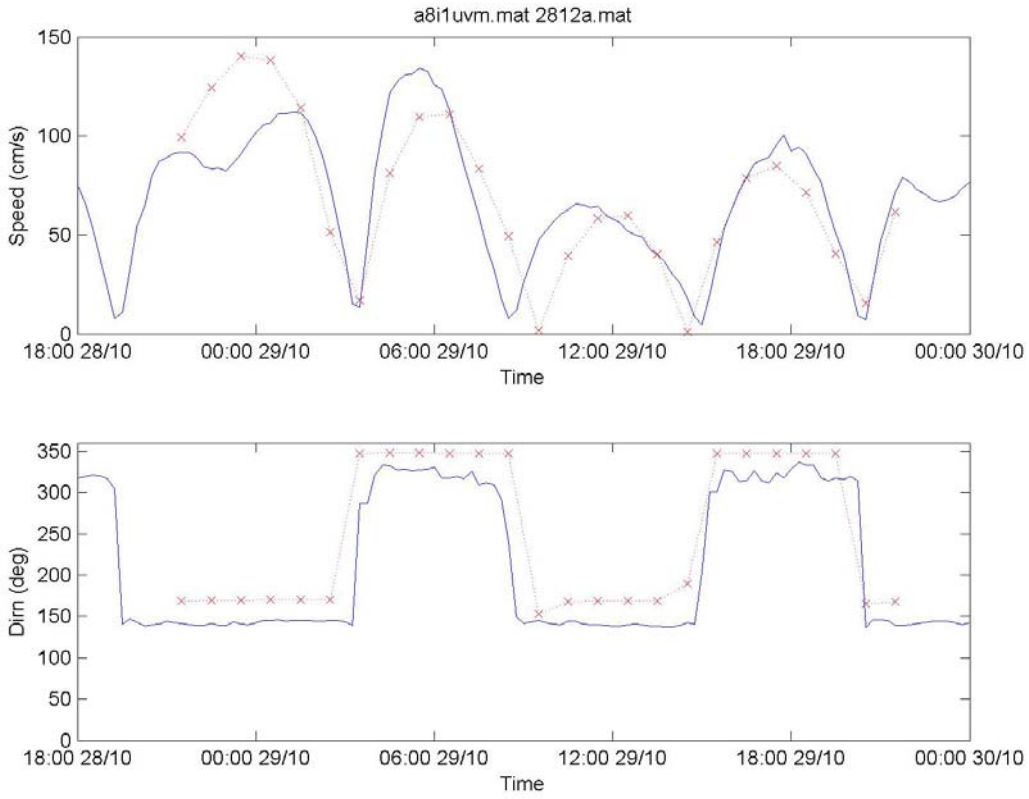

Figure 13 Scaled current speed and direction at the location of instrument A8 (Lighthouse Channel). The instrument data are indicated by the blue line; the model output by red crosses.

In the lower panel of Figure 13, there is a slight error in the current direction. This is due to the discrete nature of the model grid structure in describing the channel – note that the currents are generally in one of two directions (into or out of the lagoon). The timing of modeled direction changes is consistent with the observations. In the upper panel of Figure 13, the current speeds output by the model show good comparison with the measurements, with the exception of the period around midnight (0000 hours) on 29 October 2003. At this time, the current profile showed that the direction of the current was consistent throughout the water column except near the surface, where the magnitude was also greatly reduced. This inconsistency suggests a surface event that influenced the

depth-averaged measurement (e.g., the wake from a boat or a wind-driven component of current). As the model did not incorporate anthropogenic or wind effects, any related effects would not be reflected in the model output.

Figure 14 shows the current speed and direction, from both model and data, for the location of instrument A13 (Toachel Mid) for a 1.5-day period towards the end of the simulation. Here it can be seen that the model is unable to describe higher-frequency variations in the speed and directions, due to the one-hour temporal resolution of the model output. However, the model does provide a very good description of the low-frequency variations in the currents.

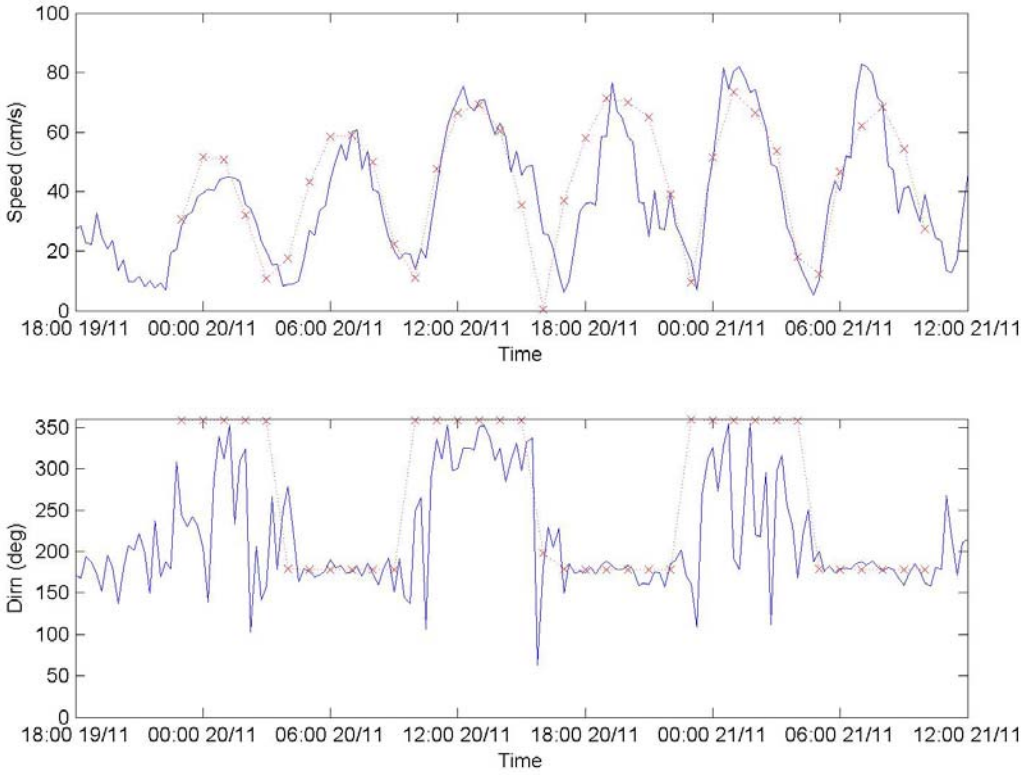

Figure 14 Scaled current speed and direction at the location of instrument A13 (Toachel Mid). The instrument data are indicated by the blue line; the model output by red crosses.

Figure 15 shows a scatter plot of scaled model output and measured current speeds at the location of instrument A8 (Lighthouse Channel) for the duration of the model. The line of equity (45° line) is also shown. Here we see that the model compares well with the data through the entire simulation.

Analyses of the model output data have shown it to be consistent with observations. The model output was employed directly in the production of the heat-stress map for Palau.

Improvement to the information gained from the hydrodynamic model requires an increase in resolution, both temporally and spatially. This in turn would require considerably higher-quality bathymetry and access to super-computer facilities to execute the model script.

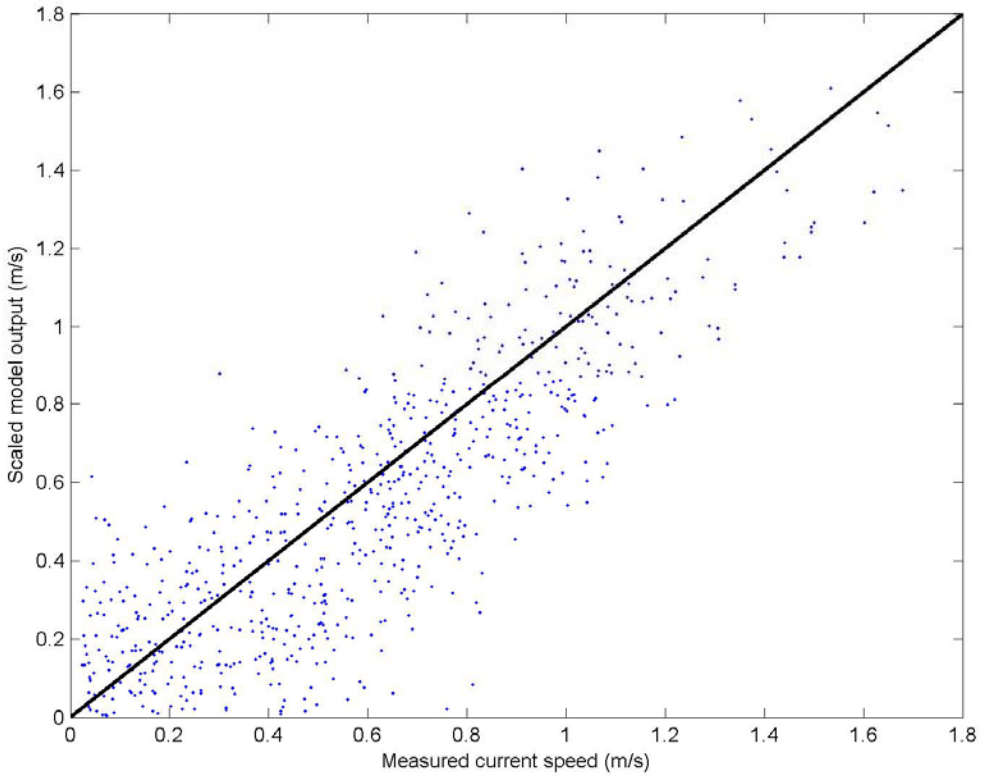

Figure 15 Scaled model output against measured current speed for location A8 (Lighthouse Channel). The solid black line is the line of equity.

Vertical temperature profile

The General Ocean Turbulence Model (GOTM) written by Burchard *et al.* (1999) is used here to calculate the vertical temperature distributions in Palau. GOTM simulates small-scale turbulence and vertical mixing in the ocean water column. It is a one dimensional, hydrostatic water column model which uses the Boussinesq approximation when calculating the turbulent eddy viscosity. GOTM allows the selection of a range of state-of-the-art turbulence closure schemes. A dimensionless stability function, a turbulent velocity scale, and turbulent macro length scale are all needed to calculate the Kolmogorov-Prandtl relations. Several zero-, one-, and two-equation models used to calculate the turbulent velocity and macro length scales, as well as various stability functions, are available in GOTM. Here we use the second moment closure scheme and the k-ε model. Further detail on the particular turbulence schemes available in GOTM can be found in Burchard (2002).

In this application we wanted to simulate the warming of the surface waters in bleaching-like conditions to gain an understanding of how much heat would be absorbed into the water column. It is impossible to predict the exact nature of the wind and solar radiation in the next bleaching event, but we already know that it will be sunny with little to no wind. If we use maximum solar radiation (i.e. assume zero cloud) and assume that it is completely still (i.e. no wind), then we get a very hot layer of water in the top 2 to 3 meters of the water column and little to no heating below this. Experience has taught us that while this is an extreme case, it is not realistic. Usually it is very sunny, but it is rarely completely cloudless; often it is very still but rarely is there absolutely no wind. After examining the small amount of information available for the Palau 1998 bleaching event it was decided to use realistic rather than extreme values of solar radiation and wind, after Bird *et al.* (2004). This meant warming the water using incoming solar radiation with a daily maximum of 940 Wm^{-2}; an average humidity of 75% and a gentle breeze of 2.6 ms^{-1} throughout the 14 day simulation period (Figure 16). The initial condition was a linear temperature profile of 28 deg C water at the surface to 25 deg C at 50m.

Figure 17 shows that over a two week period of warming, surface temperatures rose from 28 deg C to just over 32 deg C. The depth of penetration of heat layer was around 5 meters due mainly to the slight breezes and low tidal currents that were not able to produce bottom-friction induced turbulence that reaches the surface.

The resultant temperature profile can be seen in Figure 18. This was the temperature profile used for the modeling heat-stress patterns in Palau.

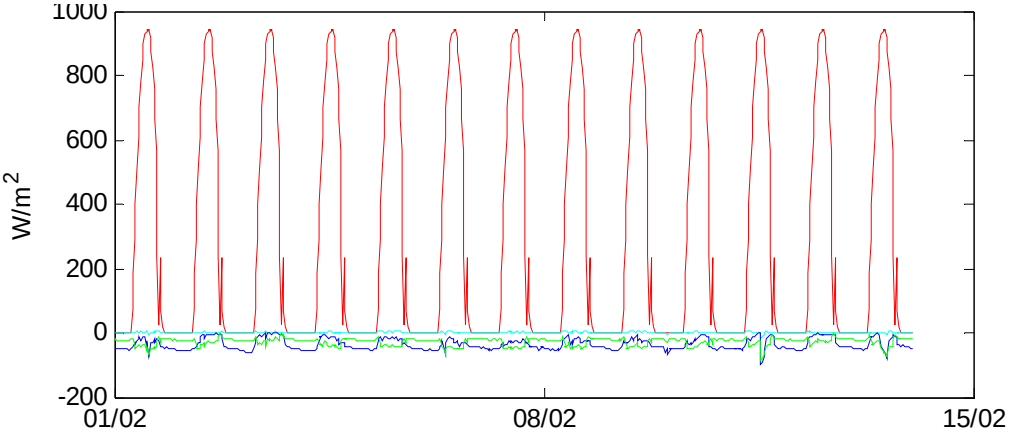

Figure 16 Plot of the heat balance: Red is incoming total short wave radiation, Green is longwave outgoing, Blue is the sensible heat flux and Turquoise the Latent Heat Flux.

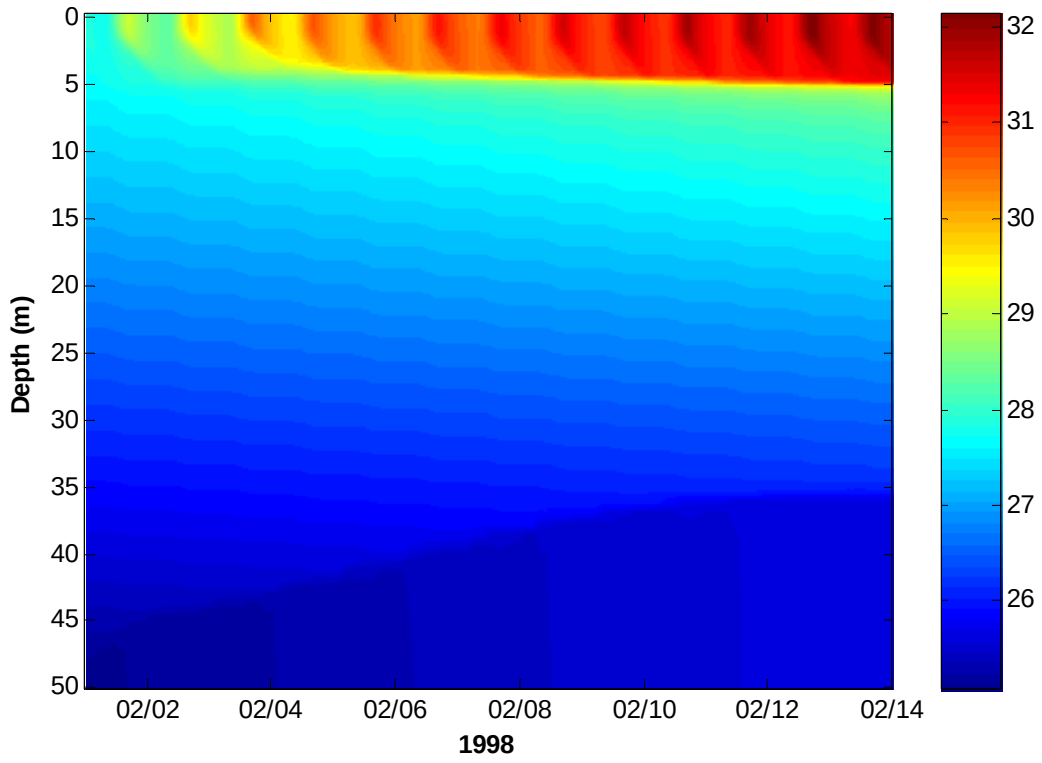

Figure 17 Development of the surface heat layer over a 14-day period.

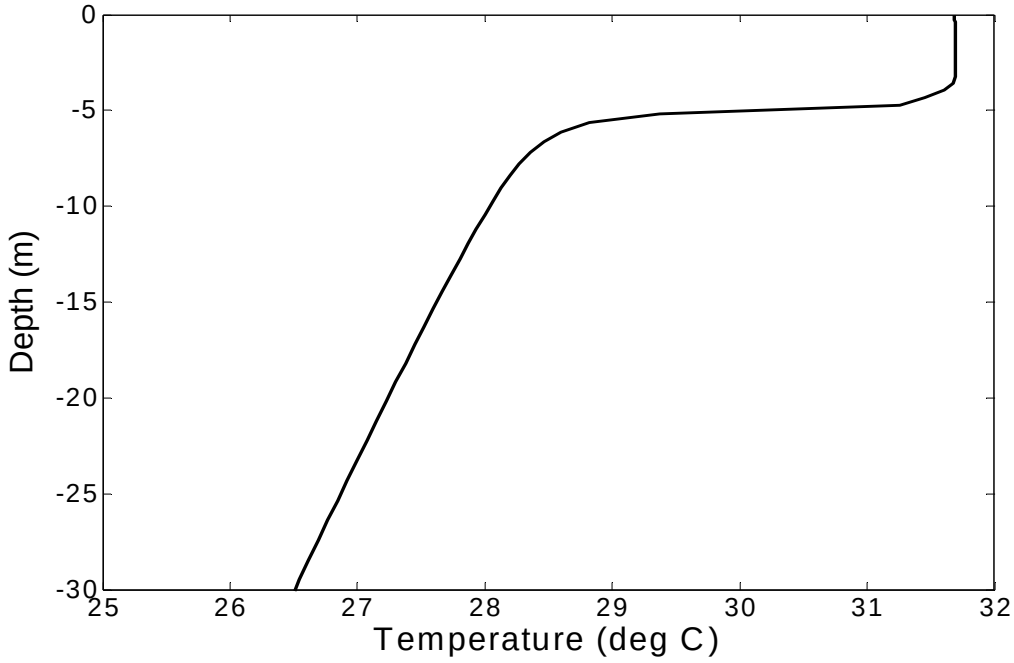

Figure 18 Vertical temperature profile on the 14th day of modeling.

Modeling heat-stress patterns during a bleaching event

Simpson and Hunter (1974) provide the parameterization that was used to distinguish between stratified and well mixed water by combining the currents with the bathymetric data (described in Heron and Skirving, 2004). See the CD for an animation (PalauModel_MixingParameter.avi) of this mixing parameter over a full tidal cycle for each time step of the model.

This information was then used in conjunction with the vertical temperature profile to determine the likely spatial distribution of sea surface temperature. For well-mixed regions, the temperature of the water column (including the SST) would be the average of the vertical temperature profile values from the surface to the local depth of water. In regions where the Simpson and Hunter (1974) parameter indicated mixing, the SST was assigned the calculated average temperature that corresponded to the local depth. All other regions were deemed to be stratified and therefore no change was made to their original 32 ^{o}C SST values.

This process forms a pattern of SST for each time step in the model, which is derived purely from mixing induced by bottom friction. Temperature changes due to advection were then added. At each time step, water from each grid point was advected according to the prescribed direction and current speed at that point. If the source water was warmer than the destination water then the destination must have been well-mixed. As such, any advected hot water to this region would then also be mixed. Given that the depth of neighboring grid points is likely to be similar, this mixed SST value would also be similar to the original destination SST.

If however the destination water was warmer than the source water then the cooler SST would prevail, since no mixing was taking place to alter the vertical thermal structure. Once this water was advected, it was heated up according to the same rate at which the GOTM model heated up the SST during the 14 day period. This would ensure that if left unmixed, the cool parcel of water would return to an SST of 32 ^{o}C within 14 days, depending on its original SST.

The SSTs were then represented as a cooling anomaly (i.e. subtract 32 ^{o}C from each SST value). See the CD for an animation (PalauModel_CoolingIndex.avi) of this anomaly over a full tidal cycle for each time step of the model.

The anomalies at each time step of the model were then accumulated in much the same way as in the methodology used to derive the NOAA HotSpot coral bleaching products (Skirving *et al.*, 2005). This methodology allowed the half hourly outputs from the model to be combined into a single map of thermal stress (Figure 19).

Potential use as a planning tool

Although good approximations, these temperatures are better used as indications of spatial patterns of relatively cooler and warmer waters during a bleaching event. In fact, this model is better described as a measure of thermal capacitance than temperature. The warmer regions have a low thermal capacitance and will heat up (and cool down) much faster than the cooler regions within the model, which have a much higher thermal capacitance.

The result of this is that the cooler regions in this model represent regions of mild thermal climatologies (i.e. less thermal stress) whereas the hottest regions represent those areas that will experience the most extreme temperatures for a region (i.e. greater thermal stress). Figure 19 is an accumulation of the final product from the Palau model. It depicts the average cooling effect accumulated over a tidal cycle (one month). The blue regions represent the most cooling at the surface due to mixing and hence represent the regions with the largest thermal capacitance. This provides the organisms that live there with a very mild climate. The red regions are the opposite.

A chart of this type can be extremely useful when designing a PAN. In general, most PANs are currently designed so as to provide protection to "representative bioregions", meaning that, as much as possible, every type of bioregion within the ecosystem of interest should be equally represented within the PAN.

An ecosystem is not only made up of different species, but it is also important to recognize that an ecosystem is also made up of organisms that have unique physiological characteristics within each species. When designing a PAN, it is relatively straight forward to map bioregions on the basis of species composition, however the unique physiological properties within each species is not represented within these techniques. With respect to a changing climate, the unique physiological characteristics are likely to be grouped into regions that will mimic the relative thermal capacitances through out the region. As a result, although we may not know what these characteristics are, the relevant characteristics for resilience against climate change can be protected if a representative amount of each thermal region within the thermal capacitance map is protected.

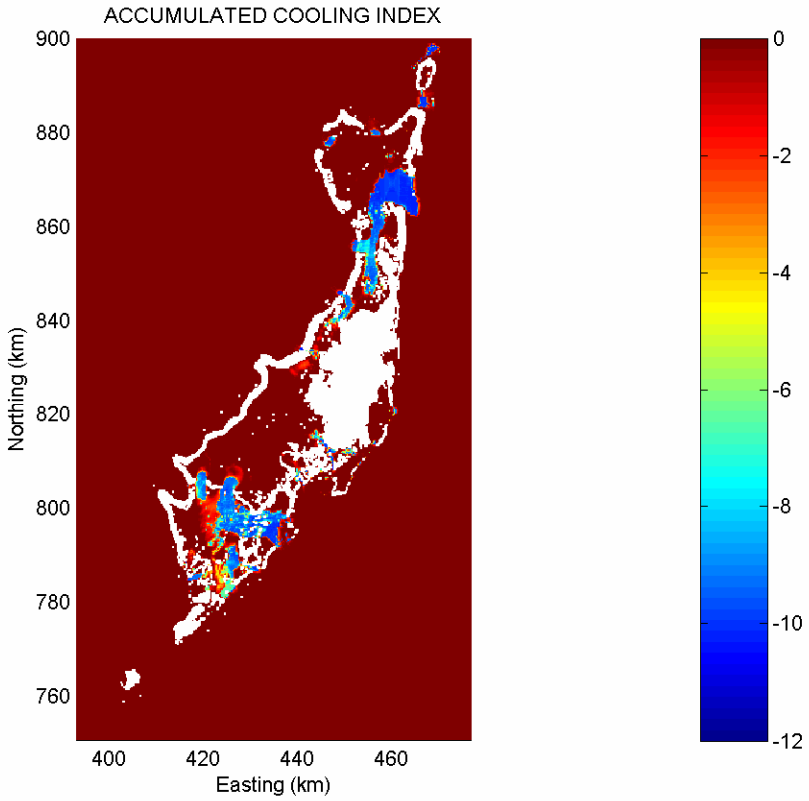

Figure 19 Final output from the Palau model of thermal capacitance, expressed as surface cooling degree-weeks (i.e. how much the mixing cooled the surface temperature during the one-month period). (from Heron and Skirving, 2004)

Summary

In 2003, NOAA and AIMS collaborated to produce a heat stress model for Palau for use in the Palau government PAN, which was being developed with the help of TNC. The idea behind this was to provide a tool that may aid the PAN designers to build in resilience against potential changes to future climate, regardless of the direction of that change.

For the model to be constructed, NOAA and AIMS derived:

1. The Palau bathymetry with a horizontal resolution of 250 meters and an rms vertical accuracy of ±1 meter.
2. A study of low frequency currents that was used to derive the seasonal low frequency currents around Palau.

3. A validated model of high frequency tidal currents.
4. A modeled vertical temperature profile.
5. An extensive suite of oceanographic validation data.

Using the bathymetry and low/high frequency currents as boundary conditions, a high resolution (250 m) two-dimensional (2-D) hydrodynamic model of the Palau region was developed to provide currents for the development of a heat stress map. Field validation data were used to assess the accuracy of the model, verifying that the model was performing well.

The Simpson and Hunter (1974) parameterization was used to distinguish between stratified and well-mixed water by combining the currents with the bathymetric data. This information was then used in conjunction with the vertical temperature profile to derive a series of thermal anomaly charts that covered an entire tidal cycle. These were then combined to produce a single chart for use with assisting the process of the PAN design.

Bibliography

Arzayus, F. and W. Skirving (2004) The correlation between ENSO and Coral Bleaching events. *10th International Coral Reef Symposium*, Okinawa, Japan, July 2004.

Berkelmans, R. (2002) Time-integrated thermal bleaching thresholds of reefs and their variation on the Great Barrier Reef. *Mar Ecol Prog Ser* **229**, 73-82.

Berkelmans, R., G. De'ath, S. Kinimonth and W. Skirving, (2004) Coral bleaching on the Great Barrier Reef: Correlation with sea surface temperature, a handle on 'patchiness' and comparison of the 1998 and 2002 events. *Coral Reefs*, **23**, 74-83.

Bird, J.C., C.R. Steinberg, T.A. Hardy, L.B. Mason, R.M. Brinkman, L. Bode (2004) Modeling Sub-Reef Scale Thermodynamics at Scott Reef, Western Australia to Predict Coral Bleaching. *10th International Coral Reef Symposium*, Okinawa, Japan, July 2004.

Blumberg, A. F. and G. L. Mellor (1987) A description of a three-dimensional coastal ocean circulation model. *In: Three-Dimensional Coastal Ocean Models, N. S. Heaps (Ed.), 1-16, American Geophysical Union*, Washington, DC.

Bruno, J.F., C.E. Siddon, J.D. Witman, P.L. Colin, and M.A. Toscano (2001) El Nino related coral bleaching in Palau, Western Caroline Islands. *Coral Reefs*, **20**, 127-136.

Burchard, H., K. Bolding, and M. R. Villarreal (1999) GOTM- A general ocean turbulence model. Theory, applications and test cases. European Commission Rep. EUR 18745 EN, 103pp.

Burchard, H., (2002) Applied turbulence modelling in marine waters, *vol. 100 of Lecture Notes in Earth Sciences*, Springer, Berlin, Heidelberg, New York, 229pp.

de Silva Samarasinghe, J.R. (1989), Transient salt-wedges in a tidal gulf: A criterion for their formation. *Estuarine, Coastal and Shelf Science*, **28**, 129-148.

Dennis, G.D. and R.I. Wicklund (1993). The relationship between environmental factors and coral bleaching at Lee Stocking Island, Bahamas in 1990. *In: Case Histories for the Colloquium and Forum on Global Aspects of Coral Reefs: Health, Hazards and History, 1993, F15-F21Glynn PW (1993). Coral reef bleaching: ecological perspectives. Coral Reefs*, **12**, 1-17.

Downs, C.A., J.E. Fauth, J.C. Halas, P. Dustan, J. Bemiss and C.M. Woodley (2002). Oxidative stress and seasonal coral bleaching. *Free Radical Biology and Medicine* **33**, 533-543.

Drollet, J.H., M. Faucon, S. Maritorena and P.M.V. Martin (1994). A survey of environmental physico-chemical parameters during a minor coral mass bleaching event in Tahiti in 1993. *Aust J Mar Freshw Res* **45**, 1149-1156.

Hearn, C.J. (1985), On the value of the mixing efficiency in the Simpson-Hunter h/u^3 criterion. Deutsche Hydrographisches Zeitschrift, **38(H.3)**, 133-145.

Heron, S.F. and W.J. Skirving (2004) Satellite bathymetry use in numerical models of ocean thermal stress. *La Revista Gayana.* **68 (2)**, 284-288.

Heron, S.F., E.J. Metzger and W.J. Skirving (*submitted*) Observations of the ocean surface circulation in the vicinity of Palau. *Submitted to Journal of Oceanography*.

Hoegh-Guldberg, O. (1999). Climate change, coral bleaching and the future of the world's coral reefs. *Mar Freshwater Res,* **50**, 839-866.

Jones, R.J., O. Hoegh-Guldberg, A.W.D. Larcum and U. Schreiber (1998). Temperature-induced beaching of corals begins with impairment of the $C0_2$ fixation mechanism in zooxanthellae. *Plant, Cell and Env,* **21**, 1219-123.

Liu, G., A.E. Strong and W.J. Skirving, (2003) Remote sensing of sea surface temperatures during 2002 Great Barrier Reef coral bleaching. *EOS,* **84**, 137-144.

Luther, D.S. and C. Wunsch (1975) Tidal Charts of the Central Pacific Ocean, *Journal of Physical Oceanography*, **5**, 222-230.

McField, M.D. (1999) Coral response during and after mass bleaching in Belize. *Bull. Mar. Sci.,* **64**, 155-172.

Newhall, R. and S. Rohmann (2003) "Using Landsat and IKONOS Imagery to Create Habitat Classifications and Mosaic Maps of Pacific Freely Associated States" *Proceedings for the 30th International Symposium on Remote Sensing of Environment. Honolulu, USA,* 10-14 November 2003, CDROM.

Simpson, J.H. and J.R. Hunter (1974) Fronts in the Irish Sea. *Nature*, **250**, 404-406.

Skirving, W.J. and J. Guinotte (2001). The sea surface temperature story on the Great Barrier Reef during the coral bleaching event of 1998. *In: Wolanski E(ed) Oceanographic process of coral Reefs: Physical and Biological Links in the Great Barrier Reef. CRC Press, Boca Raton, Florida,* 376pp.

Skirving, W.J. (2004) The Hydrodynamics of a Coral Bleaching Event: The role of satellite and CREWS measurements. In: The effects of combined sea temperature, light, and carbon dioxide on coral bleaching, settlement, and growth (J.C. Hendee, Ed.), NOAA Research Special Report, March 2004, 33-34.

Skirving, W.J., C.R. Steinberg, S.F. Heron. (2004) The hydrodynamics of a coral bleaching event. *ASLO/TOS Ocean Research 2004 Conference,* Honolulu, Hawaii, February 2004.

Skirving, W.J., A.E. Strong, G. Liu, C. Liu, F. Arzayus, J. Sapper and E. Bayler, (in press) Extreme events and perturbations of coastal ecosystems: Sea surface temperature change and coral bleaching. *Chapter 2 in Remote Sensing of Aquatic Coastal Ecosystem Processes, L.L. Richardson and E.F. LeDrew (Co-Eds), Kluwer publishers*.

Stumpf, R.P., K. Holderied and M. Sinclair (2003) "Determination of water depth with high-resolution satellite imagery over variable bottom types" *Limnology and Oceanography*, **48**, 547-556.

Wilkinson, C.R. (1998) Status of Coral Reefs of the World: 1998. *Global Coral Reef Monitoring Network and Australian Institute of Marine Science, Townsville, Australia,* 184pp.

Wilkinson, C.R. (2000) Status of Coral Reefs of the World: 2000. *Global Coral Reef Monitoring Network and Australian Institute of Marine Science, Townsville, Australia,* 363pp.

Winter A., R.S. Appeldoorn, A. Bruckner, E.H. Williams and C. Goenaga (1998). Sea surface temperatures and coral reef bleaching off La Parguera, Puerto Rico (northeastern Caribbean Sea). *Coral **Reefs*** **17**, 377-382.

Appendix 1

Steinberg, C.R., S.F. Heron, W.J. Skirving, C. McLean and S.M. Choukroun (2004) Palau Oceanographic Array Data Report, August 2003 – January 2004. *Report to The Nature Conservancy. Australian Institute of Marine Science and National Oceanic and Atmospheric Administration.* 246pp.

Appendix 2

Heron, S.F., E.J. Metzger and W.J. Skirving (*submitted*) Observations of the ocean surface circulation in the vicinity of Palau. *Submitted to Journal of Oceanography*.

Appendix 3

Heron, S.F. and W.J. Skirving (2004) Satellite bathymetry use in numerical models of ocean thermal stress. *La Revista Gayana*, **68**, (2) 284-288.